

Automated Three Stage Red Lesions Detection In Digital Color Fundus Images

C.MARIÑO, E. ARES, M.G.PENEDO, M. ORTEGA, N. BARREIRA, F. GOMEZ-ULLA[†]

Grupo de Visión Artificial y Reconocimiento de Patrones

University of A Coruña

Campus de Elviña s/n, A Coruña, 15071

SPAIN

{castormp,infmab00,mgpenedo,mortega,nbarreira}@udc.es

[†]Instituto Tecnológico de Santiago

Avenida das Burgas, 2

Santiago de Compostela, 15705

SPAIN

ciulla@usc.es

Abstract: The screening process is a very valuable method for prevention of many pathologies including Diabetic retinopathy. Typically, a large amount of images have to be analyzed as diabetic patients have both their eyes examined at least once a year. To effectively manage all this information and the workload it produces, automatic techniques for analyzing the images are required. These techniques must be robust, sensitive and specific to be implemented in real-life screening applications. In this work an algorithm for the detection of red lesions in digital color fundus photographs is proposed. The method performs in three stages: in the first stage points candidates to be red lesions are obtained by using a set of correlation filters working in different resolutions, allowing that way the detection of a wider set of points. Then, in the second stage, a region growing segmentation process rejects the points from the prior stage whose size does not fit in the red lesion pattern. Finally, in the third stage three test are applied to the output of the second stage: a shape test to remove non-circular areas, an intensity test to remove that areas belonging to the fundus of the retina and finally a test to remove the points which fall inside the vessels (only lesions outside the vessels are considered). Evaluation was performed on a test composed on images representative of those normally found in a screening set. Moreover, comparison with manually-obtained results from clinical experts are performed, to set the accuracy and reliability of the method.

Key-Words: Fundus, microaneurysm, red lesions, retina, screening, correlation.

1 Introduction

The retinal fundus photographs are widely used in the diagnosis of eye diseases, like the diabetic retinopathy. Prevalence of the diabetes among the Spanish population is 4%, about 1.6 million people [1], where about 95% of young diabetic and 78% of adult diabetic persons will present diabetic retinopathy in the next 20 years from their diagnosis, with a blindness percentage of 10% from both groups. Processing automatically a large number of retinal images can help ophthalmologists to increase the efficiency in medical environment, and prevent visual loss and blindness. This is specially useful in the diabetic screening programs organized by the different governments, where hundreds of people are examined using images from both of their eyes, captured using fundus cameras (Figure 1). Given the large number of diabetic patients screened yearly, the number of retinal images

generated is large and the majority of them is normal (typically over 90% does not present any sign of diabetic retinopathy), so an automatic mean for discarding the patients without abnormalities can reduce the workload of the doctors in a high amount, improving diabetic patient's quality of life.

One important symptom of diabetic retinopathy is the development of red lesions such as microaneurysm and white lesions such as exudates and cottonwool spots. Here only red lesions will be located, since they are among the first absolute sign of diabetic retinopathy. Several studies have been presented to deal with the problem of hard exudates detection. [2] show that using size, shape, texture, etc. in isolation is insufficient to detect hard exudates accurately. This fact is used in this work too. Several other attempts have been made to detect hard exudates using histogram segmentation. If the background color of



Fig 1: Digital color retinal image used as input for the diagnosis.

a retinal image is sufficiently uniform, a simple and effective method to separate exudates from the background is to select proper thresholds [2–4]. In [5] Mahalanobis distance is used as the classifier criteria, but results were inconclusive. Many other approximations can be found in literature, like mathematical morphology based [6, 7] or neural network based [8], with results ranging in sensitivity from 85% and specificity of 76% [9], sensitivity of 77.5% and specificity of 88.7% in [10] or sensitivity 93.1% and specificity of 71.4% [11], this last obtained using a commercially available automatic red lesion detection system.

In this work a new algorithm for the detection of red lesions is proposed. The method performs in three stages (Figure 2). In the first stage, working on the green channel of the input (color) image, several correlation filters are applied, each with a different resolution, detecting this way a wider spectrum of features and getting the initial set of candidate lesions. The output of this stage serves as input for the second stage, where a region growing process is used to preprocess the red lesion candidates set obtaining a more accurate set. Finally, in the third stage the previous set of candidates is filtered by means of four filtering processes: a shape (circularity) filter, which rejects regions with “low circularity”, an intensity filter, which removes from the set the candidates which does not fulfill the intensity criteria, a correlation mean filter, which removes the candidate areas which represent an outliers in the correlation filter response and finally a last filter which, using the creases of the digital angiography [12, 13], removes that areas inside or next to vessels. In the following sections each of these stages will be described. In section 2 description of the correlation filters of the first stage is included. Section 3 provides details on the region growing algorithm.

Once the regions have been obtained, the filtering process to discard false positives is described in section 4. Experiments and results are given in section 5 for the different stages of the algorithm, and finally section 6 provides discussion and conclusions.

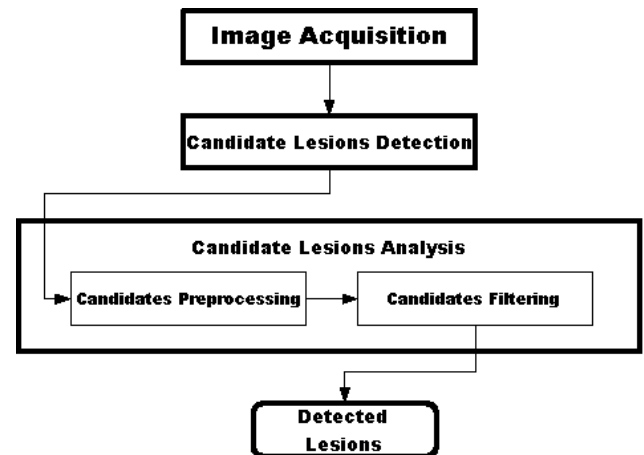


Fig 2: General schema of the proposed methodology. Once the image is acquired, the correlation filters are applied to get an initial set of candidate lesions. These candidates are analyzed, first preprocessing them using a growing regions algorithm and then applying several filters in order to obtain the final lesions set.

2 Correlation Filters Set

The goal in this stage is to get the set of candidate red lesions. Since the regions corresponding to lesions have a wide variety of sizes, three correlation filters with different resolutions, F_1 , F_2 and F_3 , are applied to the image. As proposed in [14], since red lesions have the highest contrast in the green plane [15], in place of applying the correlation to the gray-level version of the image, green plane I_g is used as the input.

Red lesions are small regions in the image with an approximately circled shape and much darker than the background (since single channel images are used the color info is discarded). Figure 3(a) shows the aspect of a typical red lesion in the green channel of the original image, with the profile in the center of the lesion depicted in 3(b).

The three images resulting from the correlation with the three filters, C_1 , C_2 and C_3 , each of size $M \times N$, are combined using equation 1, so that output from this stage R' is an image where each pixel corresponds to the maximum output value from the correlations in its location. Then, a threshold τ is applied to the output, to discard low value correlation pixels, and finally connected regions are built with the values over that threshold. The result from this process will be the candidate red lesion regions.

$$R' = \max\{C_1(x,y), C_2(x,y), C_3(x,y), \forall x,y | 1 \leq x \leq M, 1 \leq y \leq N\} \quad (1)$$

In order to design the shapes and sizes of the filter's kernels, red lesions from the images in the test set are isolated and analyzed. As it can be observed in Figure 3(b), a red lesion template can be forged using a Gaussian pattern.

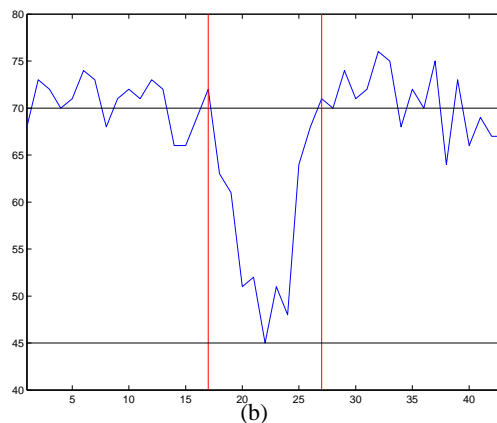
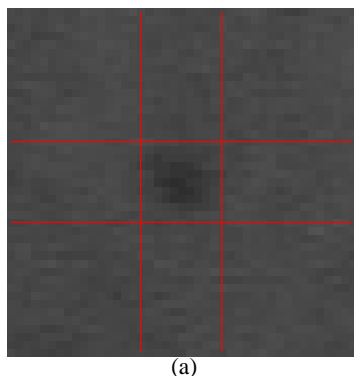


Fig 3: Green channel view of a red lesion. The pixels belonging to the lesion are darker than the background. Top: lines mark borders of the lesion, located in the centered square. Bottom: profile of the center of a red lesion.

Assuming symmetry in the red lesion, the Gaussian pattern can be described as a one-dimensional function, being the variable the distance (or radius) to the center of the lesion as showed in Equation 2.

$$f(r) = ae^{-br^2} \quad (2)$$

where parameters a and b control the shape of the generated Gaussian curve. In Figure 4 a two-dimensional Gaussian template is depicted.

But, since the red lesions have a circular shape, a second, more "ideal", template was tried to correlate with the red lesions, and results from both templates compared. The kernels of these second filters were

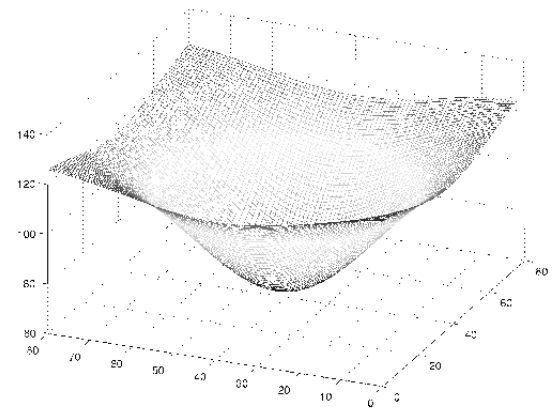


Fig 4: Example of one of the three Gaussian kernels which the image is correlated with.

designed to be again square-shaped, this time with a circle inside simulating the red lesion. Figure 5 shows one of the kernels used with this approximation.

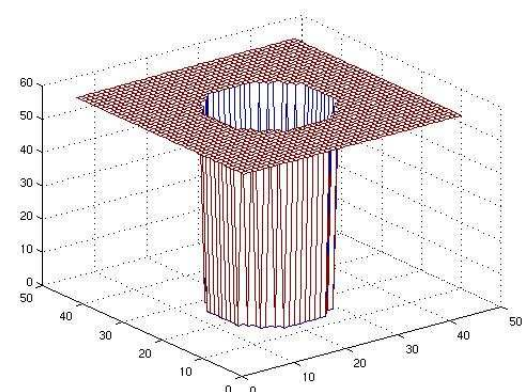


Fig 5: Example of one of the three kernels which the image is correlated with.

To set the sizes of the kernels, several numbers were tried. The best results were obtained with the sizes of the kernels, from bigger to smaller, 43, 23 and 15 pixels, both in the Gaussian and in the circular shaped kernel. In the case of the Gaussian kernel, the radius also varied, with sizes 10, 5 and 3 respectively. The threshold τ was set to 0.43, the lower value obtained from the profile of the red lesions, as showed in Figure 3(b).

Both the correlation kernels were tested with the images test set, and results are included in Table 1. Table 1 shows the early results obtained for images from patients with red lesions and images from healthy patients (no Red Lesions). These results showed an extremely good sensibility but a relatively high average

of false positives per image. Although this phase is meant to detect of all the true lesions while successive ones aim to identify them as true or false, an improvement was made in order to lower the false positive rate. But using the same test images images, the results obtained with the circular kernel template allowed to increase the correlation value threshold to 0.5 thus reducing the false positive cases

		Red Lesions	no Red Lesions
Gaussian	Sensibility	95%	N/A
	False positives	186	72
Circular	Sensibility	95%	N/A
	False positives	137	49

Table 1: Red lesions candidates detection sensibility and average false positives per image obtained using three Gaussian templates (first and second rows) and using three circular kernel templates (third and fourth rows).

Despite the meaningful reduction of false positives many areas not belonging to red lesions are obtained in this stage (Figure 6). These areas must, of course, be discarded from the result. This will be the objective of the second stage of the algorithm.

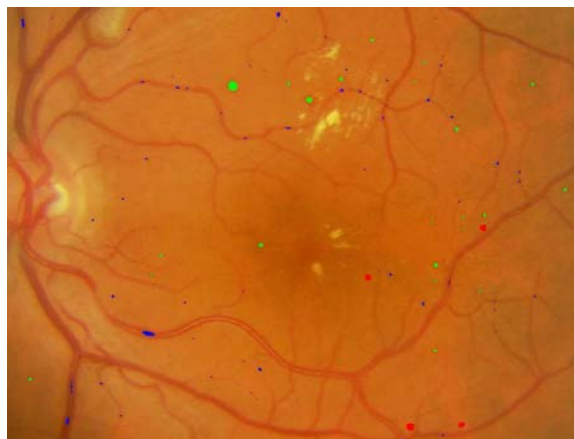


Fig 6: Cropped region from the output image after applying the correlation filters, equation 1 and thresholding to image from Figure 1. Candidate red lesions are marked in red, green and blue.

3 Region Growing Algorithm

To remove false positives from the output of the stage 1, a growing region algorithm is used. The regions which contain less than a given threshold will be removed, since they correspond to noise and false features detected as lesions. In a growing region algorithm, first step consists on finding the seeds for the growing regions. Here the point with the higher correlation value from each region output from stage one

will be considered as seed (which will be the center of the lesion, if the region comes from a lesion). Once the seed has been found, the threshold t for the growing process is determined following equation 3 [14].

$$t = i_{seed} - \alpha(i_{seed} - i_{bg}) \quad (3)$$

where i_{seed} is the intensity at the starting seed position, i_{bg} is the intensity of the same pixel in an image resulting from applying a median filter with kernel size 41×41 to I_g and $\alpha \in [0, 1]$. Here $\alpha = 0.5$. Growing starts in the seed pixel and stops when no more connected pixels below the threshold can be found. The grown objects together form the final candidate object set. If the region size is above $200px$ it will be discarded, since it will be considered as a background area or vessel area. This threshold value has been set empirically, analyzing the sizes of the red lesions in the test set of images, composed by 100 images. Figure 7 depicts the result from this stage applied to image from Figure 6.

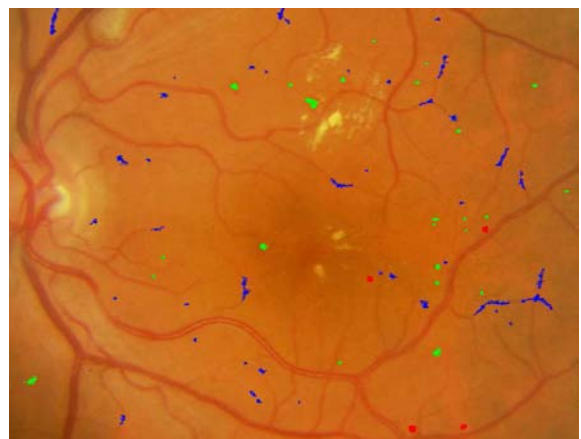


Fig 7: Cropped region from the output image after applying the growing region process to image (Figure 6). Regions are marked as green and blue areas.

Table 2 describes the quality improvement achieved in this stage comparing the false positive average obtained in section 2.

Images type	Red Lesions	no R. Lesions
Sensibility	95%	N/A
False positives	66	18

Table 2: Results obtained applying the growing region algorithm.

Image in Figure 7 shows some regions that are not red lesions, and should still be removed from results. This goal will be fulfilled by stage three of the algorithm, commented in the next section.

4 Feature Based filtering Process

In the last stage, several high-level knowledge based filters have been designed to improve detection results. This improvement is acquired by removing false positives and not doing so with the true positives.

4.1 Shape Filtering

The first applied filtering process consists on removing the regions which does not fit in the regular shape of the red lesions, which are circular shapes. In this step, the degree of circularity for each region is measured, and using a threshold, non-circular shapes are delete from the set of candidate regions. Circularity C is computed by means of equation 4.

$$C = \frac{p^2}{4\pi a} \quad (4)$$

where p represents the perimeter of the candidate region and a represents its area. Then, equation 5 is applied, in order to choose only circular-like regions.

$$Threshold(C) = \begin{cases} \geq U_t, \text{region accepted} \\ < U_t, \text{region rejected} \end{cases} \quad (5)$$

The value $U_t = 0.375$ was determined empirically by evaluating the set of test images (Figure 8). In Figure 9 the result obtained from this filter is depicted, showing the regions accepted marked as blue and green areas.

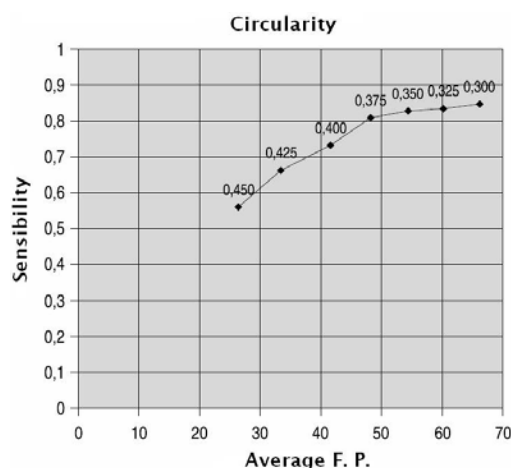


Fig 8: Sensibility and false positives values depending on the circularity threshold used.

Table 3 shows the results obtained applying the circularity filtering to the output of the growing-region algorithm stage.



Fig 9: Cropped region from the output image after applying the shape filtering process. Regions are marked as green and blue areas.

Images type	Red Lesions	no R. Lesions
Sensibility	85%	N/A
False positives	36	7

Table 3: Results obtained applying the shape filter to the output from stage one described in section 2.

4.2 Intensity Filtering

The second filtering process performed in this third stage is an intensity-based filtering. Since red lesions are dark structures, lighter structures can be removed from the set of candidate regions. Since illumination is not constant among images, a robust threshold is needed, and it can not be a constant. From the set of test images, a functional threshold was designed, so that it depends only on the mean value of the green plane image.

In each of the images, an expert clinician set the right threshold so that minimum of false positives was zero, minimizing the number of false negatives. Equation 6, the intensity threshold, I , was obtained by a minimum square error fitting of a straight line to the set of values obtained from this manual validation.

$$Threshold(I) = 0.8054\bar{I}_g + 27.3723 \quad (6)$$

where \bar{I}_g represents the mean value of the green plane of the image. Candidate regions above the threshold will be removed. In Figure 10 the result from this process is shown, with candidate regions marked as green and blue areas.

Table 4 shows the obtained intensity filtering results.



Fig 10: Cropped region from the output image after applying the intensity filtering process. Regions are marked as green and blue areas.

Images type	Red Lesions	no R. Lesions
Sensitivity	87%	N/A
False positives	35	9

Table 4: Results obtained applying the intensity filter to the output from stage one described in section 2.

4.3 Correlation Filtering

The third of the filters consists on a correlation-based filter. Taking as basis the correlation image R' from first stage, this filter remove every region whose mean value for this correlation image is not above value 0.4. This value was computed empirically from the set of test images (Figure 11).

In Figure 12 the results of the accepted and rejected regions are depicted.

In Table 5 the performance of the correlation filtering is showed.

Images type	Red Lesions	no R. Lesions
Sensitivity	81%	N/A
False positives	22	4

Table 5: Results obtained applying the correlation filtering to the output from stage one described in section 2.

4.4 Creases-based Filtering

Finally, in the last of the filtering processes the creases computed from the original digital retinal image are used as landmarks (in Figure 13 the cropped creases image of the Figure 1 is shown).

Regions intersected by creases will be removed if its mean value is over 0.25. This filter removes the regions near inside the vascular tree, which must be

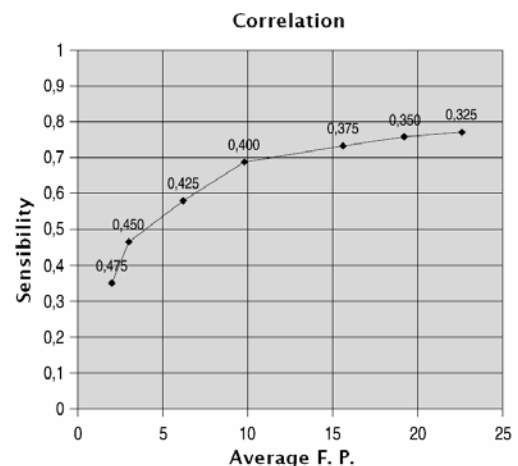


Fig 11: Sensibility and False Positives values depending on the correlation threshold used.



Fig 12: Cropped region from the output image after applying the correlation filtering process. Regions are marked as green and blue areas.

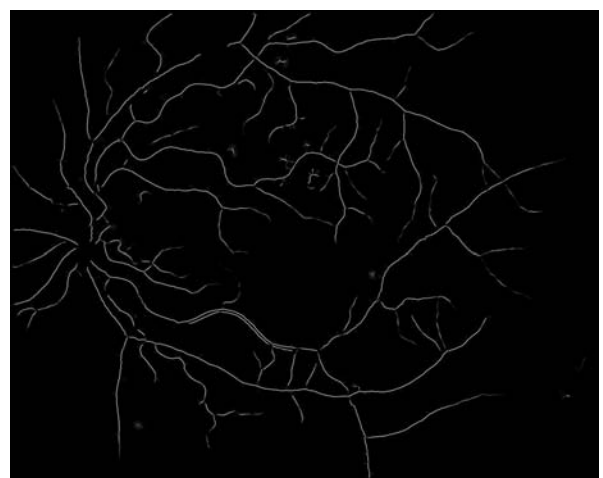


Fig 13: Creases of the cropped region of the image in Figure 1, used to remove regions inside or near vessels.

discarded in the analysis of red lesions. Figure 14 represents the variation of false positives and sensibility rate as the mean value set for removal of regions in this filter varies.

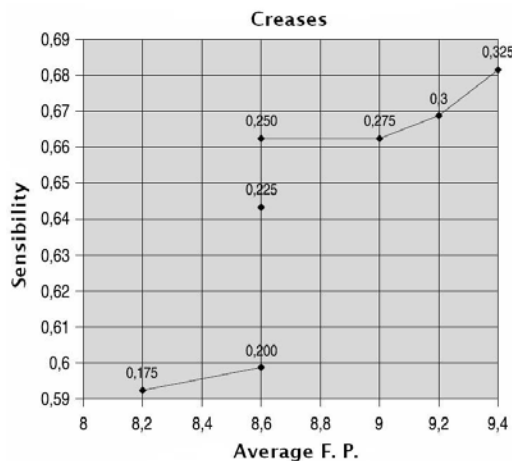


Fig 14: Sensibility and False Positives values depending on the creases threshold used.

Figure 15 depicts the output result from this filter, which is also the final result of the algorithm. Again, red lesions are marked as green and blue areas.



Fig 15: Cropped region from the output image after applying the creases-based filtering process. Regions are marked as green and blue areas.

The effectiveness of the crease-based filtering is described in Table 6.

5 Validation And Results

To validate the algorithm described in previous sections, an experiment was designed in collaboration with the oculists of the Complejo Hospitalario Universitario de Santiago (CHUS) and Instituto Tecnológico de Oftalmología de Santiago (ITO). From the set of

Images type	Red Lesions	no R. Lesions
Sensibility	85%	N/A
False positives	36	7

Table 6: Crease-based filtering results.

75 images, captured using a Canon CR5 nonmydriatic 3CCD camera at 45° field of view, the clinician manually marked the red lesions detected in 50 of the images. Then, the same images were input to the system, and obtained results were compared. 25 images without lesions were also input to the system, in order to evaluate its response to healthy people images, and to count the number of false positives. Figure 16 shows an image analyzed by the clinician, with the red lesions marked as yellow areas. To visually compare the results obtained with the algorithm described, the red lesions also detected by the system (true positives) are also rounded by a blue circle, the false positives are marked as green circles, and false negatives are marked as red circles.



Fig 16: Comparison of the manual and automatic red lesions detection in image from Figure 1. True positives are rounded by a green circle, the false positives are marked as blue circles, and false negatives are marked as red circles.

Results obtained with the whole test set of 75 images reported the numbers in Table 7, for the images with (first column) and without (second column) red lesions. First and second row show the total number of features detected (not applicable in the case of images without lesions for the manual process) for the manual segmentation and using the algorithm, respectively. In the third row the number of false positives is shown (N.A. in the case of images without red lesions). Fourth row contains the number of successfully recovered lesions, and finally fifth row displays the number of false negatives (N.A. in the case of im-

ages without red lesions).

	Images with red lesions	Images without red lesions
# candidates (manual)	1570.0	N.A.
# candidates (automatic)	1470.0	220.0
# T.P.	1040.0	N.A.
# F.P.	430.0	220.0
# F.N.	530.0	N.A.

Table 7: Numbers obtained in the evaluation of the system for the images with (first column) and without (second column) red lesions. First and second rows show the total number of features detected (not applicable, N.A., in the case of images without lesions for the manual process) for the manual segmentation and using the algorithm, respectively. In the third row the number of false positives is shown (again, N.A. in the case of images without red lesions). Fourth row contains the number of successfully recovered lesions, and finally fifth row display the number of false negatives (N.A. in the case of images without red lesions).

From the results in Table 7, it can be seen that 70.7% of the detected lesions are correctly detected, with a sensitivity of 0.785%, which compared with the results from the introduction indicates that our system could be a really helpful tool in a real screening system, reducing workload of expert clinicians by pre-filtering patients which present some kind of lesion.

6 Conclusions

In this work a system to assist in the detection of red lesions on digital retinal angiographies have been presented and validated through the whole process. The system performs in three stages: in the first stage candidate areas to be red lesions are detected by means of a set of correlation filters, adapted to different resolutions. This way features of different sizes can be detected. Then, in the second stage, a growing region algorithm together with a matched threshold allows the rejection of candidates which does not fit in the size of the red lesions. Finally, in a third stage, false positives are removed by filtering the output with four matched filters, which analyze several high level knowledge of the candidate regions: shape (searching for circularity), intensity (searching for dark areas), size (with a correlation filter) and finally discarding regions inside the vascular tree by means of the crease lines.

The whole algorithm has proven to be robust and accurate, with a sensitivity of 0.785%, although a bigger set of images and further validation is needed.

Acknowledgements: This paper has been partly funded by the Xunta de Galicia through the

grant contracts PGIDT04PXIC10501PN and PGIDT06TIC10502PR.

References

- [1] Bonafonte S. and García C.A. *Epidemiología de la retinopatía diabética*. Harcourt Brace, Madrid, 1996.
- [2] Leistriz L. and Schweitzer D. Automated detection and quantification of exudates in retinal images. *SPIE*, vol. 2298, 1994, pp. 690–696.
- [3] Ward N., Tomlinson S., and Taylor C. Image analysis of fundus photographs. The detection and measurement of exudates associated with diabetic retinopathy. *Ophthalmology*, vol. 96(1), 1989, pp. 80–86.
- [4] Philips R., Spencer T., Ross P., Sharp P., and Forrester J. Quantification of Diabetic Maculopathy by Digital Imaging of the Fundus. *Eye*, vol. 5, 1993, pp. 130–137.
- [5] Goldbaum M., Katz N., and Nelson M. The discrimination of similarly colored objects in computer images of the ocular fundus. *Investigat. Ophthalmol.*, vol. 31, 1990, pp. 617–623.
- [6] Spencer T., Olson J., McHardy K., Sharp P., and Forrester J. An image processing strategy for the segmentation and quantification in fluorescein angiograms of the ocular fundus. *Computing Biomedical Research*, vol. 29, 1996, pp. 284–302.
- [7] Cree M., Olson J., McHardy K., Sharp P., and Forrester J. A fully automated comparative microaneurysm digital detection system. *Eye*, vol. 11, 1997, pp. 622–628.
- [8] Gardner G., Keating D., Williamson T., and Elliot E. Detection of diabetic retinopathy using neural network analysis of fundus images. *Br. J. Ophthalmol.*, vol. 80(11), 1996, pp. 937–948.
- [9] Hipwell J., Strachant F., Olson J., McHardy K., Sharp P., and Forrester J. Automated detection of microaneurysms in digital red-free photographs: a diabetic retinopathy screening tool. *Diabetic Med.*, vol. 19, 2000, pp. 588–594.
- [10] Sinthanayothin C., Boyce J., Williamson T., Cook H., Mensah E., Lal S., and Usher D. Automated detection of diabetic retinopathy on digital fundus images. *Diabetic Med.*, vol. 19, 2002, pp. 105–112.
- [11] Larsen M., Godt J., Larsen N., Lund-Andersen H., Sjølie A., Agardh E., Kalm H., Grunkin M., and Owens D. Automated detection of fundus photographic red lesions in diabetic retinopathy. *Investigat. Ophthalmol. Vis. Sci.*, vol. 44(2), 2003, pp. 761–766.

- [12] López A., Lloret D., Serrat J., and Villanueva J. Multilocal Creaseness Based on the Level-Set Extrinsic Curvature. *Computer Vision and Image Understanding*, vol. 77(1), 2000, pp. 111–144.
- [13] Mariño C., Penedo M.G., Penas M., Carreira M.J., and González F. Personal authentication using digital retinal images. *Pattern Analysis and Applications*, vol. 9(1), 2006, pp. 21–33.
- [14] Niemeijer M., van Ginneken B., Stall J., Suttorp-Schulten M., and Abrámoff M. Automatic detection of red lesions in digital color fundus photographs. *IEEE Trans. Med. Imag.*, vol. 24(5), 2005, pp. 584–592.
- [15] Hoover A. and Goldbaum M. Locating the optic nerve in a retinal image using the fuzzy convergence of the blood vessels. *IEEE Trans. Med. Imag.*, vol. 22(8), 2000, pp. 951–958.